Chapter 1: Introduction & Literature Review

1.1 Introduction

Steel is a primary structural material in the automotive sector due to its high strength, durability, and cost-effectiveness. Oil crisis in 1973, marked by soaring prices and supply disruptions, prompted the automotive industry to focus on improving fuel efficiency by reducing weight of vehicle. This crisis ignited a demand for energy-efficient solutions, pushing industries, particularly steel one to concentrate on enhancing strength of it to downgauge as 10% weight reduction results in a significant 6–8% improvement in fuel efficiency [1]. As a result, advanced high-strength steels (AHSS) emerged, offering yield strength ranging from 550 MPa to over 2000 MPa. The "banana diagram" illustrating the trade-off between tensile strength and ductility across various steel grades, highlighting their evolution to meet diverse application demands is shown in Figure 1.1 [2][3]. Conventional steels, such as interstitial-free (IF), mild, and bake-hardenable (BH) steels, offer high ductility (elongation ~20–60%) but limited strength (<500 MPa), making them suitable for complex shaped parts but less load bearing applications. In contrast, high-strength low-alloy (HSLA) and ferrite-bainite (FB) steels provide enhanced strength (~400–800 MPa) with moderate elongation (~10–30%), addressing the needs of structural applications. Advanced high-strength steels (AHSS), including dual-phase (DP), complex-phase (CP), twinning-induced plasticity (TWIP), and third-generation steels, achieve superior strength (up to 1200 MPa) while maintaining balanced ductility through optimized multiphase microstructures [4], [5]. For even higher strength, ultra-high-strength steels, such as martensitic (MS) and hot-formed boron steels (MnB + HF), exceed tensile strengths of 1500 MPa but sacrifice elongation (~5–15%), making them ideal for crash-resistant components [6]. Meanwhile, austenitic stainless steels exhibit exceptional ductility (~70%)

paired with moderate strength (~400–800 MPa), finding use primarily in corrosion-resistant applications. To effectively bridge the gap between strength and ductility, AHSS grades like medium Mn steels are also under development.

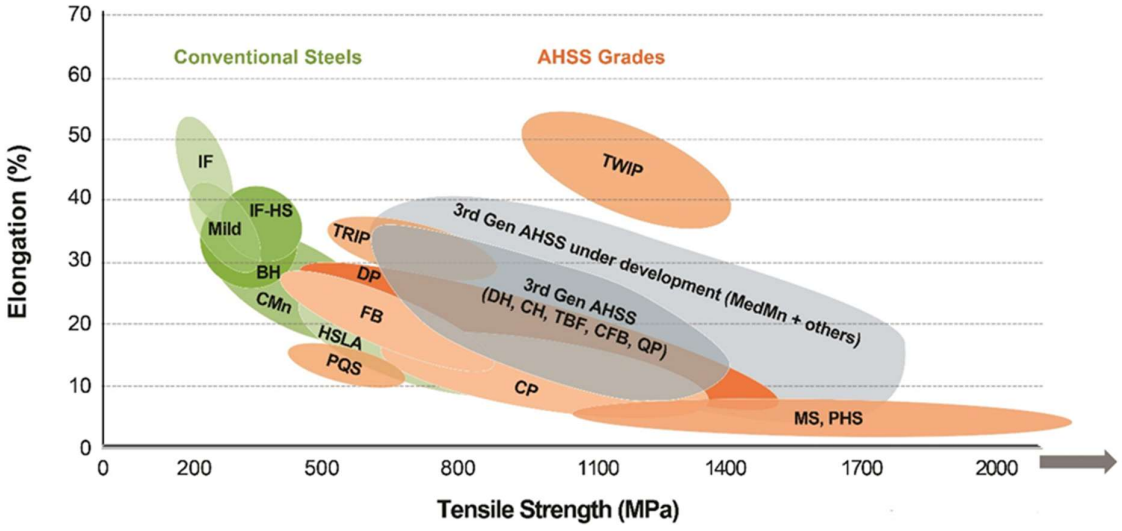

Figure 1.1: Banana Diagram depicting the strength and elongation characteristics of various steel Grades [3].

The implementation of high-strength steel allows for the use of thinner sections (Down-gauging), resulting in significant weight reduction for manufacturers while simultaneously enhancing fuel efficiency. Figure 1.2 illustrates the body-in-white structure of the 2015 Ford Edge, highlighting the mass distribution among various steel grades [7]. Notably, advanced high-strength steel grades, such as DP600, DP800, DP1000, and martensitic steels, account for 50% of the total mass distribution. Additionally, high-strength low-alloy steel grades contribute another 20%, collectively playing a significant role in mass reduction strategies.

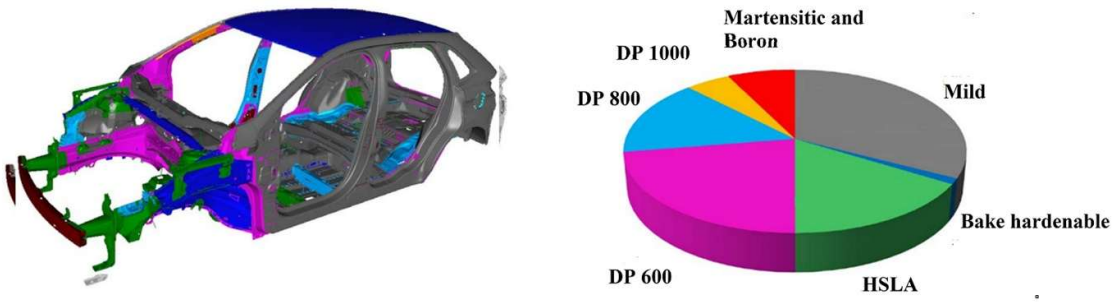

Figure 1.2: Illustrative Representation of the Body in White Structure of the 2015 Ford Edge Vehicle and the Corresponding Mass Distribution of Materials [7].

However, down-gauging presents challenges related to stiffness and lack of formability/ductility, as well as reduced material thickness can compromise structural integrity and load-bearing capacity. To address these issues, automotive and steel manufacturers are exploring alternative materials that offer comparable properties but with reduced density. The replacement of steel with magnesium (1.74 g/cc) and aluminum (2.7 g/cc) alloys can achieve weight reductions of 60% and 50%, respectively, but, their costs are approximately four times higher [8]. Additionally, Al alloys lack stiffness, and dent resistance. Similarly, Mg alloys having inferior formability and low stiffness. Because of high cost, poor dent resistance, or formability, their usages are limited to non-critical parts of 10 % only (Al alloys 9%, Mg alloys 1%) [9]. Additionally, these materials do not match the performance of advanced high-strength steel grades. At the same time, increasing concerns about greenhouse gas emissions, global regulations have imposed stricter vehicle emission standards through 2020, with even more ambitious targets set for the next decade. As, the transportation sector ranks as the second-largest contributor to global CO_2 emissions, with 78% of these emissions originating from passenger cars, trucks, and buses [10], automobile manufacturers and steel producers are actively investigating novel materials to overcome these challenges. Considering that the body structure, commonly

referred to as the "body in white," along with the chassis, accounts for 55% of the overall mass distribution in an automobile [9], these components represent the paramount opportunity for implementing lightweighting strategies. Given the challenges associated with downgauging and material substitution, researchers have focused on reducing the density of steel (7.87 g/cm³ for ferrite and 8.1 g/cm³ for austenite) itself to further decrease automobile weight without degrading mechanical properties. This is achieved by alloying the steel with aluminum. Figure 1.3 illustrates the decreasing trend in density of iron by 1.3% for every 1 mass % of aluminum addition [11]. Al increases the lattice parameter [12], thereby contributes to a reduction in density. It's lower atomic mass further facilitate density reduction.

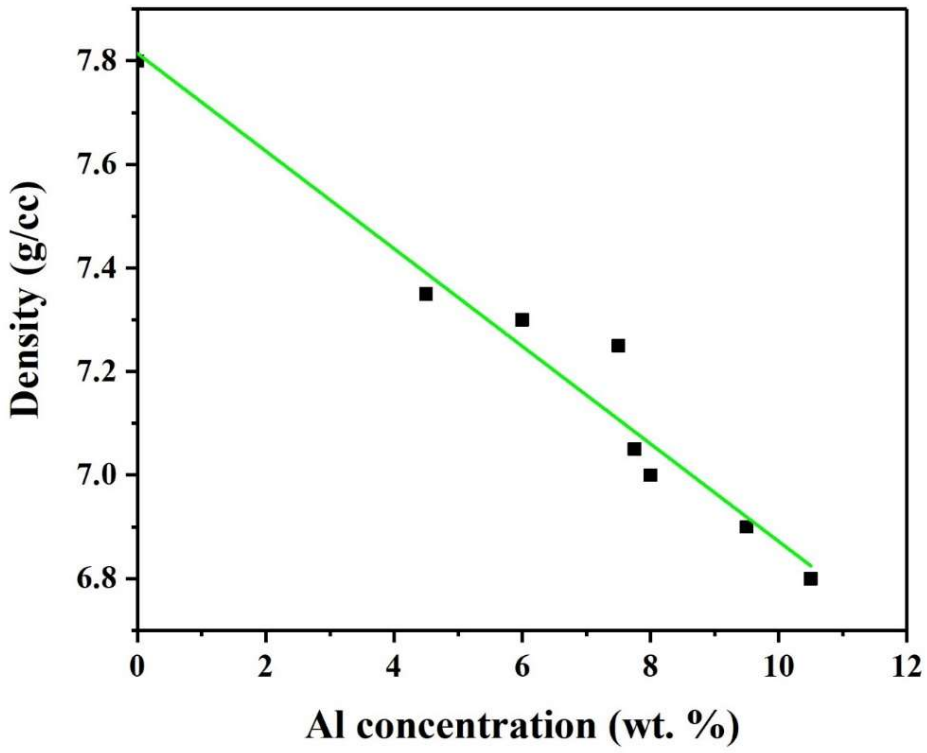

Figure 1.3: Relationship between density and aluminum concentration (mass %) in iron-aluminum alloys [11].

As Al is a ferrite stabilizer, it narrows the austenitic region, resulting in a fully ferritic structure within the 1–9 mass % Al range throughout the temperature range [13]. These ferritic steels typically contain 5–9 mass % Al, less than 5% manganese (to increase elastic modulus [14], to increase solid solution strengthening (12 MPa/1 mass %)[15]), and a minimal carbon content (<0.05%). During hot rolling, the increased recrystallization temperature of δ-ferrite due to presence of Al, causes the grains to elongate, forming band-like structures in these steels. When aluminum content exceeds 6 mass %, brittle kappa (κ) carbides form along ferrite grain boundaries, influenced by the cooling rate after hot working, reducing ductility and toughness [16]. These steels are often subjected to cold rolling, followed by recrystallization annealing typically performed in the temperature range of 700 to 1000°C to control grain size, texture, and the precipitation of kappa (κ) carbides [17]. Solid solution strengthening through aluminum incorporation is the primary mechanism for enhancing the strength of these steels, resulting in an increase of 40 MPa for each 1 mass % of aluminum content [18]. The tensile strength of these steels is comparable to that of High-Strength Low-Alloy (HSLA) steels, while their total elongation matches that of bake-hardenable steels. These steels exhibit reduced density, with ultimate tensile strengths (UTS) ranging from 200 to 600 MPa and total elongation between 10% and 40% [19], [20]. Although the density is reduced, the tensile toughness, formability [15], work hardenability remain inferior to advanced high-strength steels. Introduction of austenite in ferritic low-density steels can enhance work hardening ultimately increasing both strength, total elongation and leads to better formability. To achieve this, carbon and manganese contents were increased, resulting in the development of ferrite-based duplex steel. Ferrite-based duplex steels contain 2-12 mass % manganese and 0.05-0.5 mass % carbon, along with 5-7 mass % aluminum. In this structure, ferrite serves as the matrix, comprising more than 50%. The microstructure of these steels is characterized by austenite

grains alongside elongated delta ferrite grains at hot working temperatures. Following the hot rolling process, these steels are also cold rolled and subsequently subjected to inter critical annealing at temperatures ranging from 700 to 900°C to refine the grain size of the δ-ferrite and the γ phase and to adjust the stability and the morphology of the γ phase [21], [22]. The strength of these steels surpasses that of ferritic steels due to multiple deformation mechanisms. Initially, deformation is accommodated by the high-volume fraction of the ferrite phase, followed by the austenite phase. During later deformation, TRIP (Transformation-Induced Plasticity) or TWIP (Twinning-Induced Plasticity) mechanisms can occur, contingent upon factors like mechanical stability, stacking fault energy (SFE), and the size and orientation of austenite grains. TRIP occurs due to the lower stability of austenite resulting from lower additions of Mn content, lower SFE due to lower Al additions [20], where austenite transforms into martensite (α'-martensite) during loading [23]. Seo et al. demonstrated that in ferrite-based duplex steel with the composition Fe–5.8Mn–3.1Al–0.12C–0.47Si, austenite was retained at room temperature when annealed above 720°C. During deformation, the retained austenite transformed into α'-martensite, yielding excellent tensile strength (990 MPa) and elongation (28%) [24] . For TWIP to occur, the stacking fault energy (SFE) of the steel must range between 18 mJ/m² and 50–80 mJ/m² [25]. The addition of Al and C increases the stacking fault energy (SFE) of austenite linearly, by 10 mJ/m² per wt% of Al and 40 mJ/m² per wt% of C, respectively, while, Mn decreases the SFE in the range of 0 - 20% [25], [26]. Sohn et al. demonstrated that the Fe–0.3C–8.5Mn–5.6Al duplex lightweight steel exhibits a tensile elongation of up to 77% and a tensile strength of 734 MPa. These properties result from the concurrent formation of deformation-induced martensite and deformation twins. Additionally, plasticity is enhanced by deformation twinning in the austenite grains [27]. Thus, the tensile properties, such as tensile strength and total elongation, were improved in ferrite-based

duplex low-density steels. The tensile strength levels of these steels fall within the range of 400-1000 MPa, accompanied by a total elongation of 10-40% [19], [20]. The tensile strengths of these steels are comparable to those of Complex Phase (CP) and Duplex (DP) steels (e.g., DP 600/900) as well as TRIP steels (e.g., TRIP 450/800). Their total elongation also matches that of bake-hardenable steels [6], [20]. Although strength levels increased, the formability, total elongation, impact toughness, dent resistance, stiffness, and crash resistance remain inferior to those of conventionally used automotive grades [17], [20], [22]. To enhance these properties to levels comparable with automotive grades and further improve specific strength, the contents of Al, Mn, and C were increased, leading to the development of austenite-based steels. The following sections provide a brief literature review of austenite-based low-density steels.

1.2 Literature Review

1.2.1 Austenitic low-density steels

Austenitic steels generally consist of 5-12 % aluminum, 12-30 % manganese, and 0.6-2.0 % carbon (all by mass %) [19], [20]. In austenitic low-density steels, Al content is limited to 5-12 % to get the required density level and to prevent the formation of brittle FeAl (ordered B2) as well as to restrict the large amount of kappa carbide ($E2_1$ or $L'1_2$ perovskite-type [28]) formation [13], [20]. Manganese content is maintained above 12 % to ensure stability of austenite at low temperatures and is capped at 30 % to avoid the formation of β-Mn (A13 structure), which causes extreme brittleness [29][30], [31]. Carbon content is kept above 0.6 % to stabilize austenite but restricted to below 1.5 % to minimize the formation of excessive kappa carbide precipitates [20]. These steels are composed entirely of 100% austenite at high temperature and with the potential to stabilize austenite by rapid cooling at room temperature and facilitate the formation of κ-precipitates

by aging within the austenite grains or at the grain boundaries. Various phases coexist within this system, depending on composition and temperature, including delta (α) ferrite (BCC structure), kappa carbide, M_3C carbide, $M_{23}C_6$ carbide, M_7C_3 carbide, and β-Mn [20]. In Fe-20Mn-1C-XAl steels, addition of more than 5 % Al suppresses the formation of M_3C, $M_{23}C_6$, and M_7C_3 carbide phases, but promotes the formation of kappa carbides [32]. The increased concentration of alloying elements in these steels results in significant micro and macro segregation during solidification by slow cooling. To mitigate elemental segregation, the castings are homogenized at temperatures ranging from 1100 to 1250°C to get uniform composition without segregation. The homogenized materials are hot rolled within the single γ phase region in temperature range of 900-1100°C to break the cast structure through dynamic recrystallization. Figure 1.4 presents a schematic representation of different process variants following hot rolling, numbered 1 to 5 and depicted in distinct colours [20].

In process 1, the hot rolled plates are rapidly cooled to a temperature range of 500–750 °C to prevent the formation of brittle intergranular kappa carbides which form at grain boundaries at elevated temperatures (650-900 °C). This is followed by gradual cooling, allowing nanosized kappa carbides to form within austenite grains. The intergranular kappa carbides forms either through precipitation or cellular or eutectoid reactions, depending on the steel composition, temperature and time. Precipitation reactions typically occur within the (γ + κ) or (γ + α + κ) regions [33], [34]. Prolonged holding in the (γ + κ) region leads to the evolution of the intergranular kappa carbide (κ∗), which forms initially as discrete particles and transforms into continuous thin films along the grain boundaries of austenite (γ). In the (γ + κ + α) region, particularly at lower temperatures, both α and κ∗ nucleate independently at the austenite grain boundaries. Cellular transformation, is a distinct precipitation reaction occurs as a discontinuous process involving grain boundary

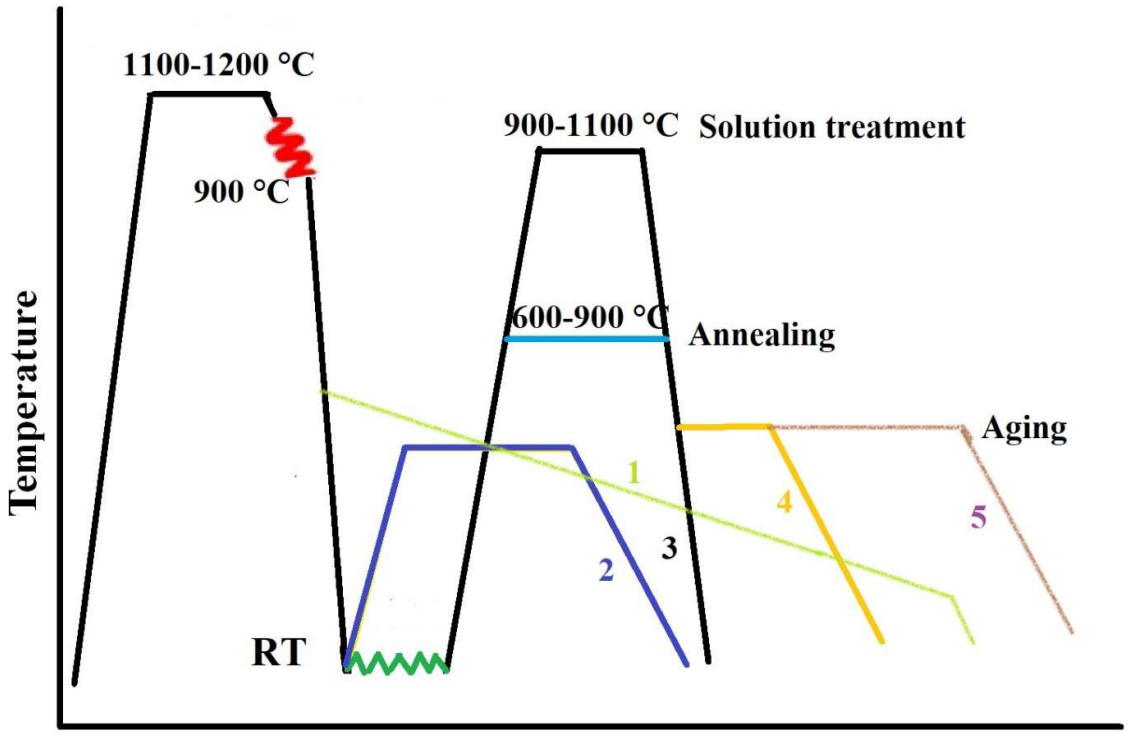

Figure 1.4: Process variants for producing austenite-based Fe-Mn-Al-C steel strips. The numbers identify process routes as described in the text [20].

migration. This transformation manifests as high-temperature austenite changes into lamellar structures comprising austenite, ferrite, and κ carbide or $M_{23}C_6$. Such reactions occur within the ($\gamma + \alpha + \kappa$) or ($\gamma + \alpha + \kappa + M_{23}C_6$) phase fields [33]. The eutectoid reaction involves the transformation of a high-temperature phase into a combination of new low-temperature phases. These carbides form when the aluminum and carbon levels surpass 5.5% and 0.7%, respectively [20]. The presence of coarser carbides negatively impacts the ductility and toughness of the steel.

Intragranular kappa carbides (κ′) forms at lower temperatures (450-650 °C), within the austenite grains. The size of κ′-carbides typically ranges from 200 to 500 Å, depending on the chemical composition, aging temperature, and aging time. Intragranular kappa carbide precipitates are coherent with the austenite matrix, exhibiting a cube-on-cube orientation

relationship characterized by [100]κ//[100]γ and [010]κ//[010]γ, with a lattice misfit of less than 3% [30], [31], [35]. Initially, the metastable κ′-carbide exhibits a cube-shaped morphology. As the annealing time increases, the accumulation of carbon (C) and aluminum (Al) atoms induces a transition to a plate-like morphology, leading to a loss of coherency. The precipitation sequence of intragranular kappa carbide from austenite (γ) can be described as follows [30], [31], [35]:

$\gamma \rightarrow \gamma' + \gamma'' \rightarrow \gamma' + L1_2\ (SRO) \rightarrow \gamma' + \kappa'$

where austenite undergoes spinodal decomposition into a solute-lean austenite phase (γ′) and a solute-rich austenite phase (γ"), where γ" subsequently transforms into the $L1_2$ structure, which then orders carbon atoms to form κ′. Intragranular precipitates occur when the aluminum and carbon contents exceed approximately 6.2% and 1.0%, respectively. Figure 1.5 (a) presents the bright-field (BF) micrograph (taken in transmission electron microscope) of intragranular kappa carbide precipitates with a rod-like morphology in the austenite matrix, and Figure 1.5 (b) provides the corresponding diffraction pattern reflecting the superlattice structures of kappa carbide, illustrating its ordered structure. Figure 1.5 (c) depicts a simulated diffraction pattern of kappa carbide relative to the austenite matrix, confirming the presence of kappa carbides. Figure 1.5 (d) features a bright-field TEM image of intergranular kappa carbide precipitates alongside ferrite, with a lamellar morphology, while Figure 1.5 (e) shows the corresponding diffraction pattern. Figure 1.5 (f) presents a simulated diffraction pattern of kappa carbide relative to ferrite, describing its relation to the ferritic phase.

In process 2, the hot-rolled plates are rapidly cooled to room temperature to prevent the formation of brittle kappa carbides. It is crucial that the cooling rate after hot rolling is sufficiently high to prevent the formation of intergranular kappa carbides. Hot rolled plates

are then subjected to isothermal aging treatment to produce fine kappa carbide precipitates within the austenite grains.

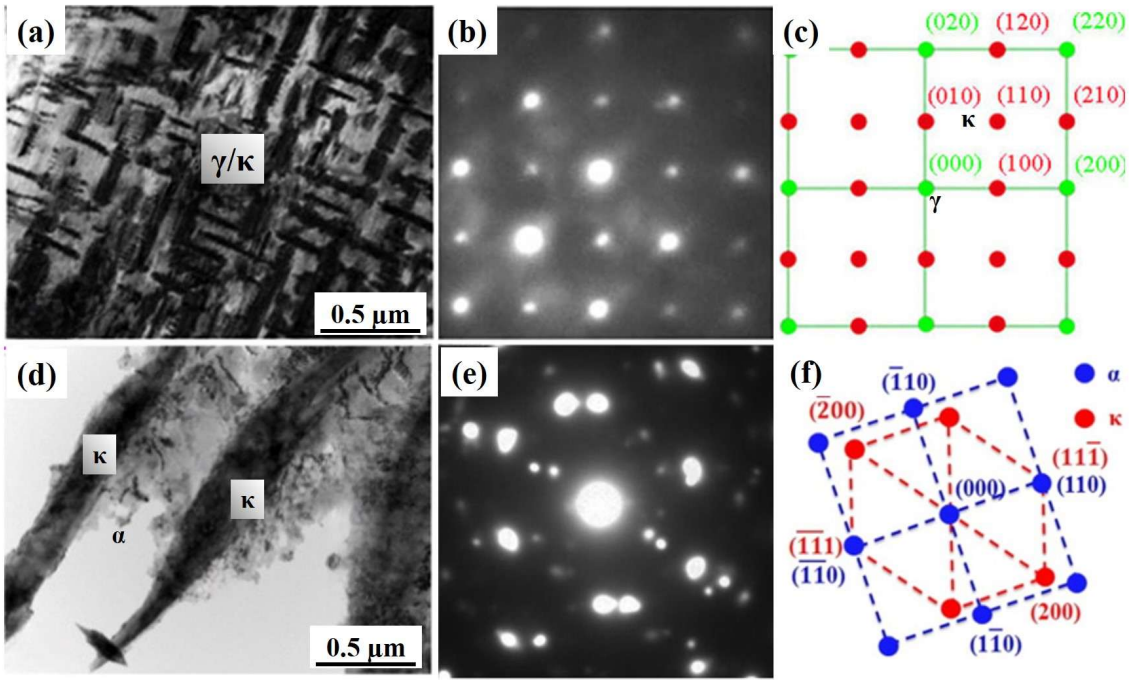

Figure 1.5: (a) TEM BF image of intra-granular kappa carbide precipitate (b) Corresponding diffraction pattern and (c) Simulated diffraction pattern of kappa carbide with respect to austenite matrix (d) Transmission electron Bright Field image of inter-granular kappa carbide precipitate along with ferrite (e) corresponding diffraction pattern (f) Simulated diffraction pattern of kappa carbide with respect to ferrite. [36], [37].

In process 3, the hot-rolled plates are air-cooled by which small amount of precipitates of kappa carbide and delta ferrite form at grain boundaries and within grains. Subsequently, the air-cooled plates are cold-rolled to a 50–80% reduction in thickness to get highest dislocation density. The cold rolled sheets are then subjected to solutionizing cum annealing treatment in the temperature range of 900–1100 °C to get recrystallized austenite grains with minimal defect density. Annealed sheets are quenched in water, oil, or other media to prevent formation of kappa carbides [38]. Park et al. demonstrated that solution-

treated and water-quenched Fe–22Mn–6Al–0.6C material, featuring austenite grains with a size of 28 ± 6 μm and annealing twins, achieves a yield strength of 317 MPa, UTS of 692 MPa, uniform elongation of 46%, and total elongation of 54% [38]. Yoo et al. demonstrated that solutionized and water-quenched Fe–28Mn–9Al–0.8C steel exhibits a yield strength of 440 MPa, UTS of 843 MPa, uniform elongation of 89%, and total elongation of 100% [39].

Further, water quenched sheets are aged in the temperature range of 450–650 °C for 5–20 hours to promote the formation of fine kappa carbides within the austenite grains, enhancing strength levels through precipitation hardening. In process 4, higher temperatures with shorter time periods are used, in process 5, lower temperatures with longer isothermal holding times are employed to maximize strength levels, albeit with the drawback of extended processing time. Choi et al. studied the aging behavior of Fe–28Mn–9Al–0.8C steel at 625°C for 3, 10, and 192 h. Nano-sized kappa carbides formed within austenite grains at all aging times, but, the 192 h aged sample exhibited coarse second-phase particles with lamellar morphology along austenite grain boundaries. The 3 h aged sample exhibited a YS of 680 MPa, UTS of 1050 MPa, and TE of 22%. The 10 h aged sample showed increased YS and UTS of 730 MPa and 1100 MPa, respectively, with a slight reduction in TE to 21.5%. The 192-hour sample displayed reduced YS (590 MPa), UTS (1000 MPa), and TE (15%) due to brittle intergranular carbides formation reducing both strength and elongation [40]. Chang et al. investigated the aging behavior of Fe–9Al–28Mn–1.8C at 450°C over durations ranging from 3 to 18 h, in 3 h intervals. The UTS increased with aging time up to 15 hours, accompanied by a reduction in elongation, while the 18-hour aged sample showed reduced UTS due to intergranular kappa carbide precipitation at austenite grain boundaries [41]. The results presented by Choi and Chang

suggest that prolonged aging, even at low temperatures, leads to intergranular kappa carbide precipitation.

For non-age-hardenable steels, the hot-rolled sheets are cold-rolled and subsequently recrystallization annealed within a temperature range of 600–900 °C for a short duration of 1–5 min to refine the austenite grains with minimal defect density or to restore ductility [42]. Jung et al. showed that recrystallization-annealed Fe-18Mn-0.6C-2.5Al PD1-Schieves a yield strength of 517 ± 8.2 MPa, UTS of 995 ± 14.3 MPa, and TE of 61 ± 1.8%, due to increased stacking fault energy from aluminum addition, promoting twinning-induced plasticity [43].

The ultimate tensile strengths of these steels range from 800 to 1500 MPa, depending on their composition and processing conditions, with total elongation varying between 30% and 80% [20]. The solution hardening effect of aluminum (Al) in austenite is limited to 10 MPa/ mass % when compared to ferrite (40 MPa/mass %) [44] [45]. The addition of carbon increases the strength of the material but reduces elongation. This effect is linked to the increased formation of κ-carbide precipitates (or ordering) in the austenite during the cooling process after the solution treatment. Adding manganese (Mn) does not play a significant role in solid solution hardening in austenite. Nevertheless, Mn can indirectly impact material properties by increasing the volume fraction of austenite and improving the solubility of aluminium (Al) and carbon (C) in the γ-solid solution. Ageing also significantly enhances the strength of these steels through the precipitation of kappa carbides. Figure 1.6 presents a comparison of the strengthening effects of various precipitates in relation to the volume fraction of kappa carbide precipitation. The analysis indicates that the strength contribution from kappa carbides can range between 100 and 350 MPa, depending on the volume fraction, which varies from 0.05 to 0.35. The engineering significance of this steel in automotive applications lies in its capacity to achieve a broad

spectrum of mechanical properties through precise control of processing conditions, without necessitating alterations to its chemical composition. For instance, water quenching results in high tensile strength and excellent ductility, while controlled cooling or short aging periods enhance yield strength with moderate ductility, providing versatility to meet diverse automotive requirements and contributing to weight reduction. Table 1.1 presents a comprehensive comparison of austenitic steels, along with their respective mechanical properties.

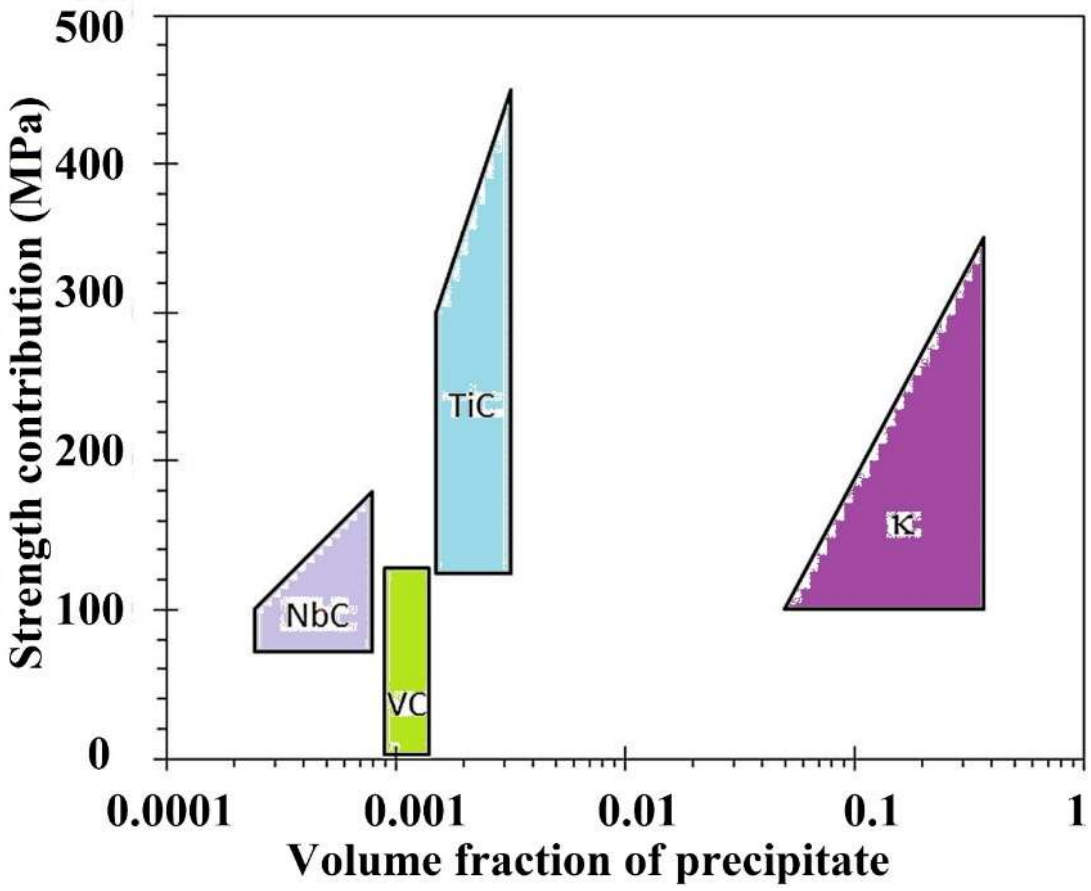

Figure 1.6: A comparative illustration depicting the impact of different precipitates on strength contribution in MPa relative to the volume fraction of kappa carbide precipitation.

Table 1.1: Mechanical properties of austenitic steels.

Alloys (in mass %)	Category	Mechanical Properties
Fe-34Mn-10Al-0.76C	Austenitic	UTS - 763MPa, YS-560Mpa and 72.5% elongation. A tensile strength of 415 MPa at 650°C is comparable to austenitic stainless steels 304 and 347 [46].
Fe-30Mn-8Al-1C	Austenitic	UTS - 890MPa, YS – 500 MPa and 54% elongation [47]
Fe-26.1Mn-10.2Al-1.02C	Austenitic	UTS – 1160MPa, YS – 1050 MPa and 25% elongation, density – 6.7g/cc and higher strength than widely used Cr-Ni steel [48]
Fe-30Mn-5Al-0.3C-0.1Nb	Austenitic	At -196°C YS- 944 MPa, which is equal to 9 mass % Ni cryogenic steels while impact energy is twice of Ni cryogenic steel. 57% elongation at -1960C. At RT 720 MPa YS and 30% elongation. [49]
Fe-28Mn-12Al-1C	Austenite+ fine nano-sized k-carbide + Ferrite	UTS- 900MPa, YS-750MPa and 55% elongation. More specific energy absorption (0.43J/mm^3) than conventionally used deep drawing steels like IF, Bake hardenable, and Thermo mechanically processed steels (0.16-0.23J/mm^3). [50]
Fe-18.1Mn-9.6Al-0.65C	Austenite based duplex	Density-6.82g/cc, UTS-1200 MPa, YS-800 MPa, TE-22%, and uniform elongation is 18%. [51]
Fe-30Mn-10Al-1C-1Si	Austenitic	YS-1300 MPa, UTS-1650MPa, 32% TE and 171J/cm2 impact energy absorbed at RT [52]
Fe-28Mn-5Al-1C	Austenitic	YS-1100 MPa, UTS- 1650 MPa, 45% elongation and 200J/cm^2 impact energy absorbed at RT equal to typical stainless steels [53]
Fe-28Mn-9Al-0.86C-0.7W-0.43Mo-0.49Nb	Austenitic	Higher no of cycles to failure than Martensitic Cr steels [29]
Fe-0.8C-16.1Mn-9.6Al-0.04Ti-0.004Nb-4.9Ni	Austenite based duplex	YS = 1357 MPa, UTS = 1548 MPa and TE = 20% YS = 1207 MPa, UTS = 1486 MPa and TE = 24% YS = 1009 MPa, UTS = 1350 MPa and TE = 32% [54]
Fe-22Mn-(7-11) Al-(0.7-1.0) C	Austenite-based duplex (Ferrite-7%)	UTS-974Mpa, TE-51%, HEC-43%, BA-152, DEH-17.2mm, ST-0.7mm. HEC is comparable to DP600 steels [55]

As shown in Table 1.1, austenitic steels typically contain higher amounts of manganese and aluminum. The high percentages of Mn. Al increase costs and cause challenges such as manganese evaporation during melting. Additionally, higher aluminum content creates issues by choking flow due to excessive oxidation during casting. Reducing aluminum content to below 7% and manganese content to below 20% may help mitigate the issues partially mentioned above. Developing a steel within this composition range while maintaining similar mechanical properties could offer advantages during melting and casting. However, only limited research has been conducted on this specific composition range [20]. Chen et al. demonstrated that the tensile properties of Fe-22Mn-7Al-0.8C steel improved after annealing for short durations at various temperatures, following a 50% thickness reduction through cold rolling. Annealing in the temperature range of 500–1000 °C, above the M_7C_3 formation temperature, partially restores ductility and yields fine recrystallised austenitic grains. Cold rolling generates numerous nanoscale twin boundaries, leading to effective grain refinement. Subsequent recovery annealing stabilises deformation twins, reduces dislocation density, and allows for cold formability and high strength through extreme grain refinement. Even though low-density austenitic steels are extensively studied for microstructure and mechanical properties, they mostly report low strength [56], [57], [58]. Austenitic steels can be strengthened through grain refinement methods like recrystallization annealing for short time, restricting grain growth by addition of reinforcements (which also increases the elastic modulus), precipitation of B2 and refinement by electropulsing. The following subsections provide a detailed review of these strengthening techniques.

1.2.2 Strengthening by grain size refinement

Usually, cold rolling followed by recrystallization annealing is adopted for strengthening and ductilization [59], [60], [61]. However, recrystallization annealing often involves

prolonged exposure to high temperatures, resulting in increased austenite grain size and reduced dislocation density. This leads to a loss of strength, despite improved elongation due to the coarser grain size. Figure 1.7 (a) demonstrates the Hall–Petch relationship in ultrafine-grained BCC steels, showing a significant increase in yield strength from 200 MPa at 50 μm to 1000 MPa at 0.2 μm. It is observed that as the grain size decreases, the yield strength of the material increases. Coarse-grained (>50 μm), fine-grained (10–50 μm), and ultrafine-grained (1–10 μm) structures are typically achieved through conventional thermomechanical treatments. However, sub-micron sized (<1 μm) grains are typically achieved through severe plastic deformation techniques like ECAP or advanced thermomechanical processes, which also elevate dislocation density, further enhancing strength. Figure 1.7 (b) highlights the grain size dependence of ductility. At larger grain sizes (150 μm), elongation is low due to anisotropic properties. Elongation improves as grain size decreases to 10 μm and remains constant between 1–10 μm. However, below 1 μm, elongation drops sharply due to reduced work hardening capacity caused by severe plastic deformation effects. To achieve an optimal balance of strength and elongation, introducing a bimodal grain size distribution while maintaining moderate dislocation density could be advantageous. In this unique structure, coarse grains contribute to improved ductility, while finer grains provide increased strength along with dislocation strengthening [62], [63]. Wang et al. demonstrated that 93% cold-rolled copper processed in a liquid nitrogen atmosphere, followed by annealing at 200°C (temperature above secondary recrystallization) for 3 min, develops a bimodal grain structure with 1-3 μm sized grains (25% volume fraction) within a matrix of ultrafine and nanocrystalline grains (<300 nm) which resulted in both enhancement in strength and recovery in ductility [63]. Similarly, Singh et al. reported that low carbon steel processed via 12 passes of equal-channel angular pressing, followed by 80% reduction in thickness through cold rolling and

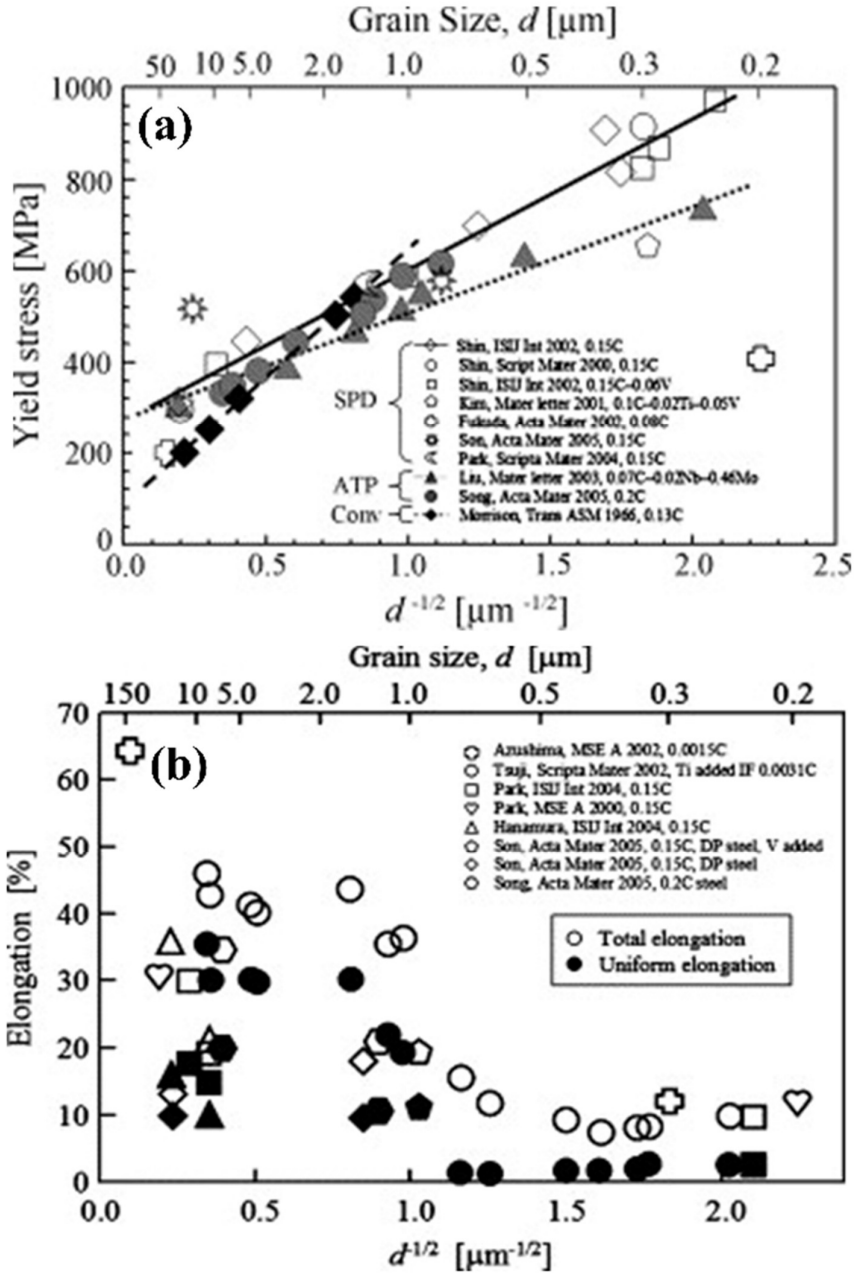

Figure 1.7: (a) Hall–Petch relationship in ultrafine grained bcc steels (b) Grain size dependence of ductility for bcc steels [64].

flash annealing at 600°C for 5 min, achieved a bimodal grain structure with ultrafine grains (size <1 μm) making up 73% of the volume and coarser grains (size ~9 μm) comprising 27%. This grain size distribution significantly enhanced strength and recovery of ductility

[62]. Thus, cold rolling followed by annealing above recrystallization temperatures for short times leads to enhanced strength and ductility combinations. Based on annealing studies on cryo-rolled copper and ultrafine-grained low-carbon steel, it can be anticipated that there is a possibility of getting bimodal grain size distribution by short annealing above the recrystallization temperature of selected austenitic low-density steel to achieve both high strength with high ductility.

1.2.3 Elastic modulus improvement

Although strength enhancement through grain size refinement can be achieved, the elastic modulus of these austenitic low-density steels remains low due to the addition of aluminum, which reduces the elastic modulus (Figure 1.8). To successfully incorporate

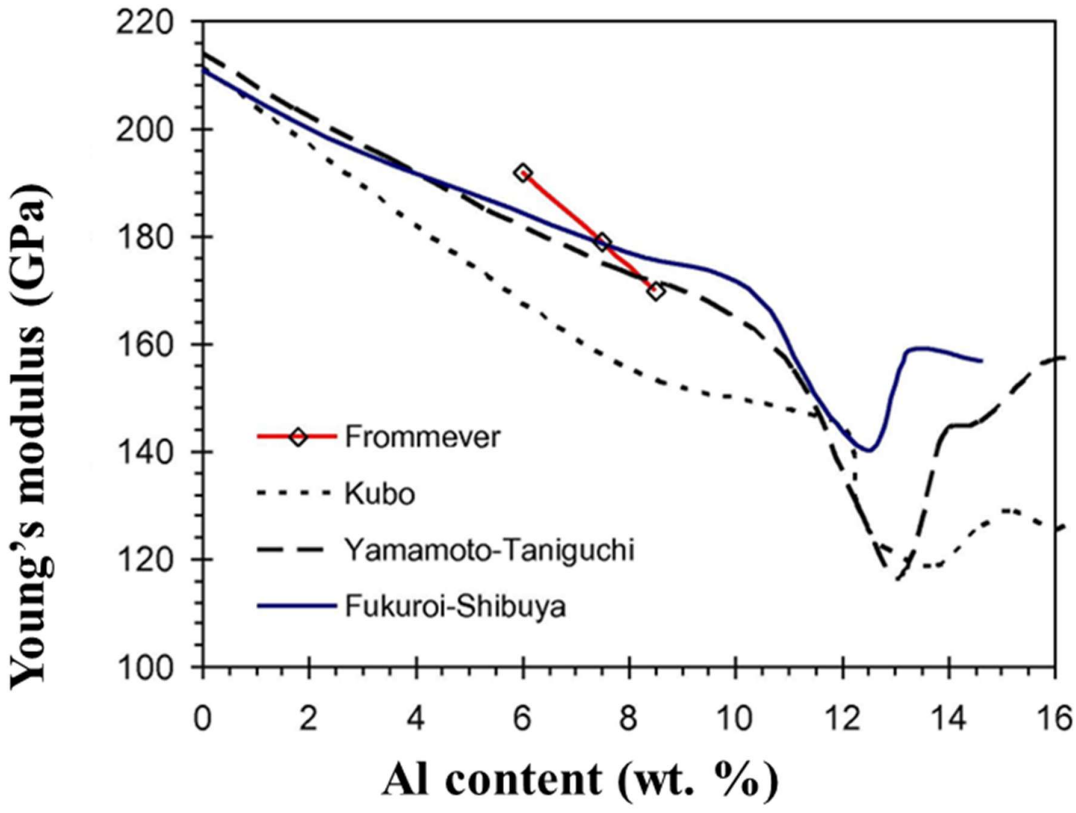

Figure 1.8: Effect of aluminum content on Young's Modulus of low-density steels.

these steels into automotive applications, the enhancement of modulus, which directly affects specific stiffness, is crucial. The addition of just 1 mass % aluminum results in a notable reduction of 2-2.5% in Young's Modulus [20]. This reduction occurs due to the decrease in the lattice energy of the Fe-Al solid solution and the increased distance between the coexisting Fe and Al atoms in the lattice. Among alloying elements Cr and Si can increase the modulus of elasticity but both are ferrite stabilizers and ferrite is detrimental for the ductility/formability which are essential for shaping the automotive parts [14]. Other than alloying additions, there are two viable approaches to enhance the stiffness of material: texture design at the crystallographic scale and the composite effect at the microstructure scale. In texture design, the goal is to employ precise thermo-mechanical treatments on carefully optimized chemical compositions to create preferential crystallographic orientations throughout the thickness of material. On the other hand, the composite effect involves increasing stiffness by introducing high-modulus reinforcement particles into the steel matrix. Texture design introduces anisotropy in Young's Modulus, whereas the composite effect results in greater isotropic properties [65]. The composite effect approach incorporates reinforcements typically possess a high Young's Modulus and low-density, improving overall stiffness. Table 1.2 presents some commonly used reinforcements in steel matrices like carbides (e.g., B_4C, SiC, TiC, NbC, ZrC), borides (TiB_2), Nitrides (AlN, BN, Si_3N_4, TiN) and oxides (Al_2O_3, SiO_2), with their elastic modulus, stiffness, and melting points [66], [67], [68]. Incorporating fine, lightweight particulate reinforcements into liquid steel presents a fascinating challenge due to their tendency to float and agglomerate, driven by low density and poor wetting properties. This makes in-situ formation of reinforcements not just a solution but a necessity for unlocking their full potential.

Table 1.2: Properties of Commonly Used Ceramic Reinforcements and Metallic Matrix Materials.

Material	Density (ρ) (g/cm^3)	Young's Modulus (E) (GPa)	E/ρ ($GPa \cdot cm^3/g$)	Melting Point (°C)
AlN	3.05	315	103	2200
Al_2O_3	3.99	400	100	2063
B_4C	2.52	450	179	2450
BN	3.48	720	207	2300
NbC	7.6	580	76	3500
SiC	3.2	480	150	2200
Si_3N_4	3.44	210	61	1750
SiO_2	2.33	100	43	1729
TiC	4.93	400	81	3067
TiB_2	4.50	370	82	2900
TiN	5.21	250	48	2950
VC	5.5	280	51	2950
ZrC	6.5	380	58	3535

By leveraging protective atmospheres during processing, the formation of undesirable oxides is effectively prevented. While AlN might seem promising, its formation is impractical because aluminum is already present, and introducing nitrogen requires high-pressure conditions, an intricate process demanding advanced expertise to avoid exposing the melt to the atmosphere. This narrows the focus to carbides and borides as viable options. Among these, the stiffness is higher for B_4C, followed by SiC, TiB_2, TiC, ZrC,

and VC. Yet, B_4C formation in liquid melts is prohibitively challenging, and TiB_2 cannot form in situ due to the superior stability of TiC. Thus, TiC stands out due to its exceptional hardness, low-density, strong bonding, chemical inertness, and high melting point [69]. Metal matrix composites with a relatively low volume fraction of reinforcement, ranging from 5% to 30%, are commonly employed in structural applications. Bonnet et al., found that TiC reinforcement increases Young's Modulus of iron [65]. There is no experimental evidence of extend of recovery in modulus in austenitic low-density steel by the addition of TiC. Furthermore, the presence of TiC leads to an increase in strength levels by inhibiting grain growth, thereby promoting grain refinement.

1.2.4 Strengthening by precipitation of α (B2)

To achieve strength levels exceeding 1 GPa, Kim et al. alloyed 5% Ni with Fe–10%Al–15%Mn–0.8%C, resulting in the formation of ordered B2 structures. This enhanced the UTS to 1350 MPa while maintaining an impressive 30% elongation after annealing at 900°C for 15 min. Nickel enhances the hardness of the B2 phase by substituting Fe-Al bonds with stronger Ni-Al bonds. These nickel-modified steels outperformed several high-specific-strength alloys like press hardened steels, Al 2000 series and Ti6Al4V, with their enhanced work-hardening of ~340 MPa, attributed to the presence of non-shearable, incoherent B2 precipitates [54], [70]. Figure 1.9 shows austenite alongside different types of B2 precipitates. Since 2015, researchers have concentrated on characterizing nickel-added low-density steels, particularly those based on Fe-Mn-Al-C alloys. Rahnama et al. investigated the mechanical properties of two duplex low-density steels (Fe-15Mn-10Al-0.8C and Fe-15Mn-10Al-0.8C-5Ni) through nano indentation, revealing that 5 mass% Ni addition significantly enhances hardness by forming stronger Ni-Al bonds in the B2 phase, at different annealing temperatures [71].

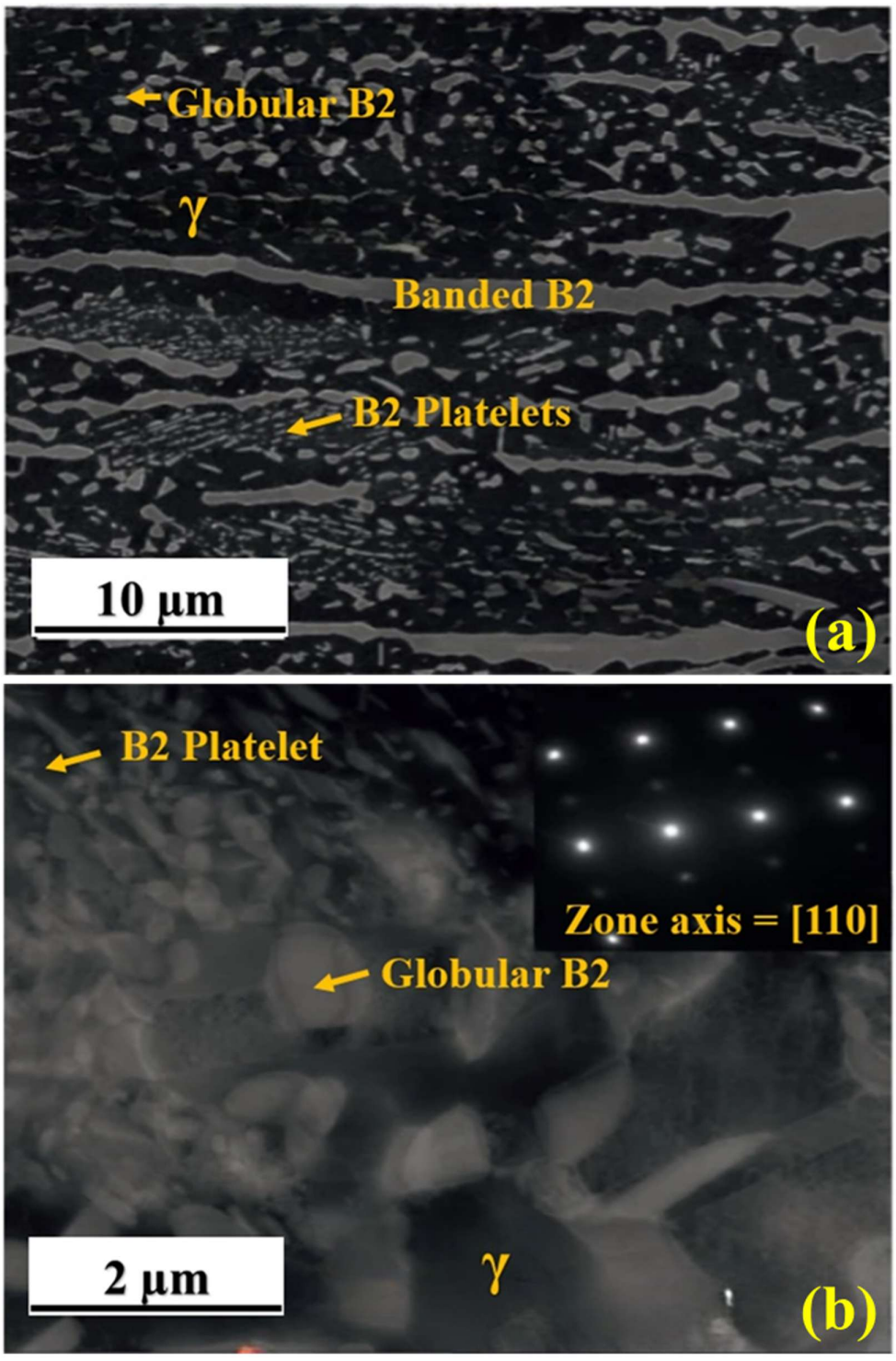

Figure 1.9: (a) SEM micrograph of different types of B2 precipitates in austenite matrix (b) TEM micrograph and corresponding diffraction pattern of B2 along zone axis of [110] [54].

In another study, Rahnama et al., found with increasing annealing temperature from 900°C to 1050°C amount of B2 deceases from 38% to 11% in Ni-added steel but higher temperatures lead to the formation of nano-sized disk-shaped B2 particles, which enhance strength and ductility compared to micro-sized faceted particles at low temperature [72]. Park et al. found that the addition of an increased amount of aluminum from 8% to 10% results in banded morphology of B2 which is responsible for improved tensile strength from 965 MPa to 971 MPa [73]. A more homogeneous microstructure with fine B2 particles in Fe-16Mn-8Al-1C-5Ni enhances ductility, and formability as well as product of strength and elongation (PSE), despite having lower strength than that of the banded B2 containing steel of Fe-15Mn-10Al-0.8C-5Ni. Yang et al. found an extraordinary strain hardening rate in Fe-16Mn-10Al-0.86C-5Ni steel due to high back stresses arising from strain incompatibility caused by the microstructural heterogeneity of B2 and austenite phases [74]. Wang et al. enhanced the strength of nickel-added high carbon and high Mn steels up to 1700 MPa through dual nano precipitation of B2 and kappa carbide via cold rolling and short-time annealing [75]. Zargaran et al. addressed the challenge of controlling B2 phase morphology in hot-rolled lightweight steels by using κ-carbide nanoparticles to promote B2 formation, resulting in uniformly distributed 13% B2 nanoparticles (20-500 nm) within the austenite matrix [76]. Mishra et al. reported that Ni-free Fe-Mn-Al-C low-density steels with fine κ-carbides had better ductility compared to Ni-containing steels with coarser κ-carbides and 12% B2 phases, which had higher strength but lower ductility [77]. Bhan et al. showed that the strain hardening is driven by lattice friction and dislocation strengthening in the γ-matrix of Fe–0.8C–15Mn–10Al–5Ni alloy [78]. Hwang et al. found fine dispersion of κ-carbide, and $D0_3$ particles in an aged alloy of Fe-21Mn-10Al-1C-5Ni, which had undergone hot rolling followed by cold rolling and short annealing that resulted in uniform distribution of globular 14% B2 near grain boundary. Such microstructure

collectively achieved an ultrahigh yield strength of 1600 MPa and a total elongation of 20 % [70]. Jia et al. showed that the addition of 5%Ni in a Fe–21Mn–10Al–1C steel and hot-rolling followed by air-cooling, promoted 10% B2 phase formation and nanosized kappa carbide which refined γ grain size by pinning that resulted in high yield strength of 1482 MPa [79]. Table 1.3 presents various nickel-added low-density steels, detailing their microstructures and corresponding properties.

Table 1.3: Processing, microstructure, and tensile properties of Ni-added low-density steels.

S. No	Composition	Processing	YS (MPa)	UTS (MPa)	El. (%)	Ref (Y).
1	Fe-16.1Mn-9.6Al-0.86C-4.9Ni-0.04Ti-0.004Nb	H + HR +CR (66%) + An				[54]
		at 900°C (2 min)	1357	1548	20.3	(2015)
		900°C (8 min)	1207	1486	24.7	
		900°C (15 min)	1009	1350	31.8	
		870°C (15 min) γ, B2 bands,	1186	1473	25.6	
		B2(200–1,000 nm), B2 platelet (50–300 nm), density 6.8g/cc				
2	Fe-15Mn-10Al-0.8C-5Ni	HR+ sol. (1250 °C for 35 min) + WQ, An at 500 °C, (γ +B2 (2-7 nm) + κ (<100nm) +B2 bands)	950	960	10.2	[72]
		700 °C, (γ +B2 (2-7 nm) + κ (<150 nm) +B2 bands)	970	980	9.8	(2017)
		900 °C, (γ + B2 (2-7 nm, 38%) + disk like B2 (200 nm) +B2 bands)	1160	1335	10.4	
		1050 °C γ + B2 (2-4 nm, 11%)	1190	1350	22	
3	Fe-15Mn-10Al-0.8C-5Ni	HR + sol (1250 °C for 35 min) + WQ				[71]
		900 °C(γ + B2 (2-7 nm, 38%) + disk like B2 (200nm) +B2 bands, H 7.9 GPa)				(2018)
		1050 °C(γ + B2 (2-4 nm, 11%) +κ <100nm) +B2 bands, H 8.5 GPa)				
4	Fe-16.3Mn-7.8Al-1.00C-4.9Ni	H+ HR+ An+ CR+ An 900 ° γ + B2 (350 nm) +B2	965	1278	31.7	[73]
		(60 nm), total 9% B2 (15 min), RD, TD	947	1231	35.5	(2019)
5	14.5Mn-9.4Al-0.73C-4.8Ni	H+ HR + CR + An 900 °C (15 min), γ + globular B2 (350 nm) + B2 (60 nm) + B2 bands, total 28% B2, RD, TD	971	1215	35.9	[73]
			1001	1234	25.2	(2019)
6	Fe-29.18Mn-8.82Al-1.2C-6Ni	H + HR + CR(60%) +An				
		800 °C (3 min) γ + 1%B2 + κ)	1600	1700	13	
		850 °C (3 min), (γ + B2 + κ)	1400	1580	21	[75]

		900 °C (3 min) (γ + B2 + κ), density 6.53 g/cc	1200	1400	38	(2020)
7	Fe-20.7Mn-9.5Al-1.0C-4.7Ni	H+ HR + CR(67%) + An				[70]
		900 °C (2 min)(γ + 10% B2)	1446	15071	24.3	(2020)
		aging 550°C (10 min)(γ + B2+ κ)	1600	622	20.2	
		900 °C (15 min)(γ + 14% B2)	1196	1372	35	
		aging 550°C (10 min)(γ + B2+ κ) , density 6.79 g/cc,	1379	1485	30	
8	Fe-20.7Mn-9.5Al-1.0C-4.7Ni	H + HR+ An, 900 °C (15 min)(γ + polygonal B2 (500 nm, 13%) + platelet B2)	1097	1397	30	[76]
		An 900 °C (15 min) + aging 550 °C (10 min), γ + polygonal B2 (2-4 nm) + platelet B2 + intergranular κ (100 nm), density 6.85 g/cc	1273	1516	25	(2021)
9	Fe-28.1Mn-8.6Al-0.9C-4.8Ni	H+ HR(85%)+air cooling, γ + κ + intergranular 4% B2 particles +DO3	730	1028	55	[77] (2022)
10	Fe-14.7Mn-9.8Al-0.9C-4.1Ni	H+ HR(85%), γ + κ + intergranular 12% B2 particles+ B2 stringers + DO3	1110	1260	20	[77] (2022)
11	Fe-28.1Mn-8.6Al-0.9C-4.8Ni	H+ HR(85%) + CR(50%) +An				
		700 °C (1 h), (γ + B2 + κ)	1450	1645	5	[80]
		750 °C (1 h)(γ + B2 + κ)	1289	1537	17	(2022)
		900 °C (1 h)(γ + B2)	900	1236	39	
12	Fe-14.7Mn-9.8Al-0.9C-4.1Ni	H+ HR(85%) + CR(50%) +An	971	1303	36	[80]
		900 °C (1 h), γ + 9% B2				(2022)
13	Fe–15Mn–10Al–0.8C–5Ni	H + HR(1 RPM) + CR(33%) + An				
		900 °C (5 min), γ + 35%B2	620	1185	15	[78]
		900 °C (15 min), γ + B2	880	1171	17	(2023)
		900 °C (30 min), γ + B2	790	1000	15	
		For 10 RPM)				
		900 °C (5 min), γ + B2	960	1160	20	
		900 °C (15 min), γ + B2	920	1150	25	
		900 °C (30 min), γ + B2	880	1120	27	
14	Fe-21.53Mn-10.08Al-0.98C-4.9Ni	H + HF + An(1100 °C for 4 h) + HR(900-1050°C), air cooling γ + 10%B2 + κ	1482	1535	23.3	[79] (2024)
15	Fe–28.3Mn–11.1Al–1.1C–4.5Ni	H+HF+sol 1200°C (1 h)+ aging	800	1242	38	[81]
		900°C (15 min), γ + 5.1% B2, density 6.6 g/cc				(2024)
16	Fe–28.3Mn–11.1Al–1.1C–4.5Ni	H+ HF+ sol 1200°C (1 h) + CR5% + aging , 900°C (15 min)	1100	1298	20	[82]
		CR10% + aging, 900°C (15 min)	1150	1330	25	(2024)
		CR 20% + aging, 900°C (15 min), γ + B2, density 6.6 g/cc	1200	1345	15	

H=homogenization, HR=hot rolling, CR=cold rolling, An =annealing, HF=hot forging, k=kappa carbide

Unfortunately, in most of the cases quantitative information about volume fraction and size of B2 phase is not available to corelate to properties of low-density steels. Further up to maximum 5% Ni was added in most of the duplex low-density steels containing 18-20% Mn. In nickel added low-density steels, previous research has predominantly concentrated on investigating cold-rolled products [74], [75], while a limited number of studies have explored only hot-rolled products [83]. Hot-rolled steels, although exhibiting lower levels of strength compared to their cold-rolled counterparts, offer the cost advantage of avoiding additional process stages. During the rolling of stated Fe-Mn-Al-C-Ni alloys, B2 nucleates at shear, deformation bands, and grain boundaries of austenite. In hot rolled materials, such nucleation sites are eliminated by continued dynamic recrystallization of the matrix. Achieving a uniform B2 precipitation and effectively controlling the microstructure in hot-rolled low-density steels poses a significant challenge due to the difficulty that arises from the continuous dynamic recrystallization that commonly takes place in materials with high stacking fault energy at elevated temperatures, as well as the larger grain sizes inherent in hot-rolled steels. So far about a maximum of 5 mass% Ni is added in austenite-based duplex low-density steels. Only in one composition, 6% Ni is added in a triplex (austenite + B2 + k carbide) steel (Table 1.3). It is worth studying duplex low-density steel of high Ni content to get increased amount of B2 precipitates to achieve high strength and hardness. Additionally, these nickel-added low-density steels can further be strengthened through electropulsing treatment by refining the B2 and austenite grains. The following section provides a detailed review of strengthening through electropulsing treatment.

1.2.5 Strengthening through electropulsing treatment

Electropulsing is a high current density (>10^3 A/cm^2) processing technique with a short time frame (microseconds) which induces changes in microstructure and properties of materials [84]. These materials include copper, titanium, magnesium alloys, aluminum

alloys, tungsten, steels, shape memory alloys, amorphous crystals and metallic glass [85]. The influence of electropulsing on the properties and performance of metallic materials is governed by their initial microstructure, crystal orientation, crystallinity, and deformation level, leading to varied effects on their mechanical properties and overall performance. Zhou et al. demonstrated that applying an electric pulse with a current density of 10.5 kA/mm² to low-carbon steel (0.07 mass % C) significantly increased tensile strength by 79% (from 580 MPa to 1040 MPa) and improved elongation by 12.5% (from 40% to 45%), attributed to the formation of a bulk ultrafine-grain microstructure with a size of ferrite grain of 0.5–3 μm after electropulsing treatment [86]. Lu et al. demonstrated that pulsed electric current (5.67×10^9 A/m², 110 μs) on 50% cold-rolled DP600 steel increased yield strength by 39%, tensile strength by 9%, and slightly reduced elongation by 5.74%. The improvement was due to ultrafine-grained ferrite with nano-cementite formation, driven by accelerated dislocation migration and enhanced ferrite nucleation during recrystallization [87]. Wang et al. demonstrated that applying a current density of 3.5 A/mm² to Aermet100 steel significantly altered the morphology of fine acicular $(Cr, Mo)_2C$ phases, transforming them into spherical (Cr, Mo)C phases [88]. Shan et al. demonstrated that electropulsing treatment (EPT) with a current density of 3.66×10^9 A/m² effectively produces a near-spherical $Mg_{17}Al_{12}$ phase (~300 nm) and a uniform ultrafine-grained structure (~900 nm) in AZ61 alloy plates [89]. Tian et al. demonstrated that applying a current density of 9.1×10^7 A/m² to annealed Ti-15-333 sheets, refines the β grains, precipitates fine intragranular α plates during aging, and suppresses continuous α grain boundary formation [90]. Jiang et al. demonstrated that applying a current density of 30.7 A/mm² leads to rapid spheroidization and dissolution of the β phase (β-$Mg_{17}Al_{12}$) in aged Mg–9Al–1Zn alloy strip. This transformation is attributed to the reduction in the nucleation thermodynamic barrier and the enhancement of atomic diffusion [91]. Further

electropulsing technique is utilized to dissolve high-temperature $Mg_{17}Al_{12}$ precipitate in AZ91 [92] , β-Mg2Si in AA6061 [93], at a much lower temperature than the respective thermodynamic equilibrium temperature to reduce its size, to accelerate uniform precipitation of T-phase, $Al_{20}Cu_2Mn_3$, in AA2024 [94] , Ni_3(Ti, Mo) in a maraging steel [95], to control both size and size distribution. RA Fard has demonstrated that the application of electropulsing to low-carbon steel results in a reduction in the size of precipitates [96].

As stated earlier, conventional processes like homogenization and hot rolling at 1200–900°C, while reducing oxidation and tool wear, fail to refine the coarse banded and globular B2 phase due to the low processing temperatures. While combinations of homogenization, hot rolling, cold rolling, annealing, and aging treatments promote additional B2 and kappa carbide precipitation, the morphology and size of high-temperature B2 phases remain largely unchanged. Thus, it is anticipated based on the above literature that application of electropulsing treatments on this nickel added austenitic low-density steel, promotes the dissolution of high-temperature coarse B2 precipitates, refinement of the microstructure, spheroidization of B2, and a more uniform distribution of B2 precipitates, which further increases the strength levels.

1.2.6 Ductilization through electropulsing

Electropulsing treatment not only enhances strength but can also improve ductility in certain metals, albeit with a slight reduction in strength. Magargee et al. reported that applying an electropulse with a current density of 6 A/mm² reduced the ultimate tensile strength of commercially pure titanium from 520 MPa to 490 MPa, while elongation increased from 25% to 33%, attributed to the electroplasticity effect [97]. Several theories explain the electroplasticity effect. Troitskii suggested that it arises from the interaction of electrons with dislocations, which increases dislocation mobility due to the higher velocity

of electrons [98]. Song et al. observed that electric pulse with current density of 7.22 kA/mm^2 significantly recovered the ductility of the material, increasing elongation from 10% to 37% in cold-rolled sheets of commercial TA1-A CP titanium. They attributed this improvement to the formation of fine equiaxed grains and a lamellar microstructure induced by electropulsing, which reduced the effective slip distance and enhanced flow stress through the Hall–Petch mechanism [99]. In another study by Song et al. on TC4 titanium alloys, electropulsing treatment increased tensile elongation by 35%, while yield strength decreased by 19.8%. This improvement was attributed to recrystallization, restrained grain growth, and a decrease in dislocation density due to the drifting of electrons [100]. Zhu et al. showed that pulse electric current increased the elongation of deformed ZA22 alloy by 437%, due to accelerated dislocation movement [101]. In the case of AZ91 alloy, electropulsing treatment following cold rolling significantly recovered ductility, increasing it by 91% [102]. Rehanama et al. studied 0.14 mass % C TRIP PD1-Snd observed a 13% increase in elongation after applying an electric pulse with a peak current density of 1.018×10^7 A/m^2. This was accompanied by a 15.79% reduction in yield and ultimate tensile strength, attributed to lamellar refinement, spheroidized structure formation, and reduced interlamellar spacing [103]. Lu et al. reported that electropulsing treatment on Fe-26Mn-9Al-0.75C, reduced the volume fraction of kappa carbides and facilitated their fragmentation, transitioning the microstructure from lamellar to spherical morphologies [37].

In nickel-added low-density steels, the inherently brittle nature of B2 and kappa carbide phases often compromises ductility despite high strength levels. Refining these phases and achieving a uniform distribution of precipitates could enhance elongation without significantly reducing strength, thereby improving the overall mechanical performance of these alloys. Thus, there is a possibility to refine high temperature B2 precipitation by

partially dissolving it, improvement in uniformity of distribution, modification of non-spherical B2 precipitates to spherical B2 precipitates, and reduction in dislocation density by recrystallization annealing, which may further improve the ductility of the nickel added low density steels.

1.3 Objectives of the present investigation

Based on the detailed literature review and shortfalls, the objectives of the present thesis are to design austenitic, and austenite based duplex low-density steels of high strength, elastic modulus and ductility through microstructural modification by thermomechanical treatments and electropulsing treatment, incorporation of reinforcement. The present thesis is aimed at:

- designing austenitic and austenite based duplex steels to achieve low-density.
- investigating the impact of thermal cyclic treatment on the microstructure and tensile properties of austenitic low-density steel.
- designing a TiC reinforced austenite matrix composite for improvement in modulus of elasticity.
- standardizing thermomechanical process parameters to achieve high strength in nickel added low-density duplex steel.
- refining and redistributing the B2 precipitates for improvement in strength-ductility combinations through electropulsing treatment in nickel added low-density duplex steel.